Simultaneous Application of Pressure-Infusion-Gyration to Generate Polymeric Nanofibers

Xianze Hong, Suntharavathanan Mahalingam, Mohan Edirisinghe*

Polymeric nanofibers are a fascinating class of material that has been widely used in a myriad of applications, including fiber reinforced composites, protective clothing, and chemical sensors. Here, the science of the combined application of external pressure, controlled infusion of polymer solution and gyration, which allows mass production of uniform polymeric nanofibers in a single step, is uncovered. Using poly(ethylene oxide) as an example this study shows the use of this novel method to fabricate polymeric nanofibers and nanofibrous mats under different combinations of processing parameters such as working pressure (1×10^5 to 3×10^5 Pa), rotational speed (10 000–36 000 rpm), infusion rate (500–5000 μL min^{-1}), and fiber collection distance (4–15 cm). The morphologies of the nanofibers are characterized using scanning electron microscopy and anisotropy of alignment of fiber is studied using 2D fast Fourier transform analysis. A correlation between the product morphology and the processing parameters is established. The produced fibers are in a range of 50–850 nm at an orifice-to-collector distance of 10 cm. The results indicate that the pressure coupled infusion gyration (PCIG) offers a facile way for forming nanofibers and nanofiber assemblies.

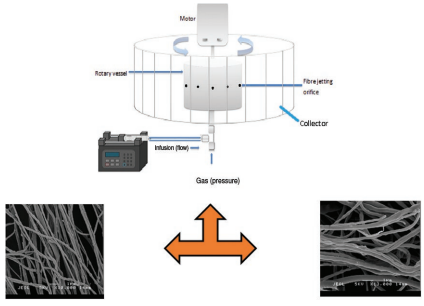

1. Introduction

The production of nanofibers has recently garnered much attention due to their unique features including large surface area-to-volume ratio and superior mechanical properties, which renders them captivating in potential applications like catalyst supports, tissue engineered scaffolds, and functional group delivery vehicles (e.g., for drugs).[1–16] The superior features of a well-aligned structure of fibers compared to nonwoven (randomly arranged) fibers makes them an optimal candidate in applications such as composite reinforcements, basement for differentiation of peripheral nerves and tendon cells, and other applications which require a particular orientation.[17–20] Despite the surge of interest in nanofibers, major challenges still restrict their implementation due to lack of a high production rate.

Until recently, template synthesis related processes,[20] molecular self-assembly,[21] and electrospinning[22–25] have been used as the most common methods used to fabricate ultrafine fibers, with the latter being the most popular technique. Despite the versatility of the electrospinning method, its utilization is strikingly limited by significant challenges including: (1) increased cost and safety concern induced by application of high-voltage electric fields; (2) limited selection of materials due to sensitivity

X. Hong, Dr. S. Mahalingam, Prof. M. Edirisinghe
Department of Mechanical Engineering
University College London (UCL)
Torrington Place, London WC1E 7JE, UK
E-mail: m.edirisinghe@ucl.ac.uk

to solution electrical conductivity; (3) random orientation of obtained fibers; (4) commercial viability hampered by its low production rate. Although a scheme of nozzle-free electrospinning as well as multiple spinning setups[22] have been implemented to improve the fiber production yield, these strategies further increase the production cost of this technique.

Recently, some techniques that utilize centrifugal force to produce fibers on a large scale have attracted a great deal of interest. These methods jet out polymer solution or melt using a high velocity air stream to produce nanofiber. For example, centrifugal rotary spinning,[26,27] force spinning,[28] pressurized gyration,[3,29–31] and infusion gyration[32] are shown to be effective ways to eliminate the aforementioned limitations encountered by electrospinning. These methods make uniaxially aligned 3D fibrous bundles from solutions or melt in a cylindrical spinneret by utilizing centrifugal force reliably, consistently, and cost-effectively. Our previous studies demonstrated that pressurized gyration and infusion gyration are simple methods largely independent of materials properties from which various products can be effectively produced, for example, fibers with nanoparticles,[33] microbubbles,[31] especially well-aligned biopolymer nanofibers[34] and hybrid products[32] (with functional groups, e.g., peptide, nanoparticles) in a very short time. Pressureless gyration and centrifugal spinning are able to produce fibers consistently with an induced solution flow, but usually only generate uniform fibers in the range of sub-micrometer to micrometer scale.

In this work, we invent and investigate a complementary spinning process, a pressure coupled infusion gyration (PCIG) spinning system to produce nanofibers with diameters ranging from 60 to 850 nm with a high yield. Poly(ethylene oxide) (PEO) is a well-known basic polymer with good mechanical properties and good biocompatibility, and is used as an example to demonstrate the characterization of this new process. Thus, we investigated the feasibility of producing PEO nanofibers by utilizing the newly developed facile system. In PCIG, the spinnability of a polymer solution is highly affected by its rheological properties, especially the chain entanglement in the polymer solution. The dimensions and the homogeneity of nanofibers are controlled by the polymer solution properties. Furthermore, the size, distribution, and morphology of nanofibers are governed by the processing parameters. Hence, orifice-to-collector distance, rotational speed, working pressure, and infusion rate were varied and their effects were evaluated together with polymer concentration. The resultant nanofiber morphology was characterized using field emission scanning electron microscopy (FE-SEM); a quantitative measurement of anisotropy of produced fiber alignment was performed by 2D fast Fourier transform (2D FFT) analysis as a function of spinning conditions. Various concentrations of PEO polymer solutions were used, and they were spun based on implementing 144 different combinations of key processing parameters available in the PCIG process in order to study the effects on fiber morphology.

2. Experimental Section

2.1. Materials

PEO with a molecular weight (M_w) of 2×10^5 g mol^{-1} purchased from Sigma-Aldrich (Poole, UK) was used as-received and deionized water was selected as the solvent. It has a relatively slow evaporation rate compared to other volatile solvents such as ethanol. Five different weight percentages (3, 5, 10, 15, and 21 wt%) of PEO were dissolved in deionized water. These five solutions were magnetically stirred at the ambient temperature (25 °C) for 24 h to obtain homogeneous solutions before processing. For comparative purposes, the concentrations of PEO chosen in this work are similar to a previous work on the pressurized gyration[3] and infusion gyration.[32] The viscosities of the six solutions were measured at 21 °C with a Brookfield DV-III ultraprogrammable rheometer (Brookfield Viscometers Ltd., Harlow, UK), the apparent shear rate spanned the range 0.013–26.4 s^{-1}.

2.2. Pressure Coupled Infusion Gyration

PCIG system (see Figure 1) used in this work consists of a rotational vessel—60 mm in diameter and 40 mm in height. The vessel was equipped with 20 orifices equidistantly located on the wall of the vessel at the same height, and each ≈0.5 mm in diameter. Nanofiber's geometry and cross section can be affected by the features of vessel and orifices (geometry and size), which could be customized. The vessel is driven by a DC motor which connects at the top of the vessel, and it could provide various rotating speeds up to 36 000 rpm. The applied pressure (up to 3×10^5 Pa) was provided by a nitrogen cylinder connected to the bottom of the vessel. A syringe pump connected by a plastic tube via a T-junction to the bottom of the vessel is used to control polymer solution flow (up to 5000 μL min^{-1}) and continuously feeds into the vessel during processing. A stationary copper mesh served as the collector. It was placed around the vessel and helps convenient collection of fibers. During rotational spinning, PCIG effectively utilizes high speed rotation of the vessel to extrude several solution jets parallely out from orifices that are located on the vessel surface.

PCIG utilizes continuously injected solution flow and high rotational speed which allows effective use of materials and quick fiber generation, and at increased flow rates can dramatically improve the yield of fiber production. The vessel is powered by a DC motor and the rotational speed was controlled in this study in the range from 10 000 to 36 000 rpm by a speed control panel. A syringe pump (Harvard Apparatus Ltd., Edenbridge, UK) with a 10 mL syringe was used to feed a polymer solution into the vessel simultaneously during rotation, and the injection flow rate was set at six different values (500, 1000, 2000, 3000, 4000, and

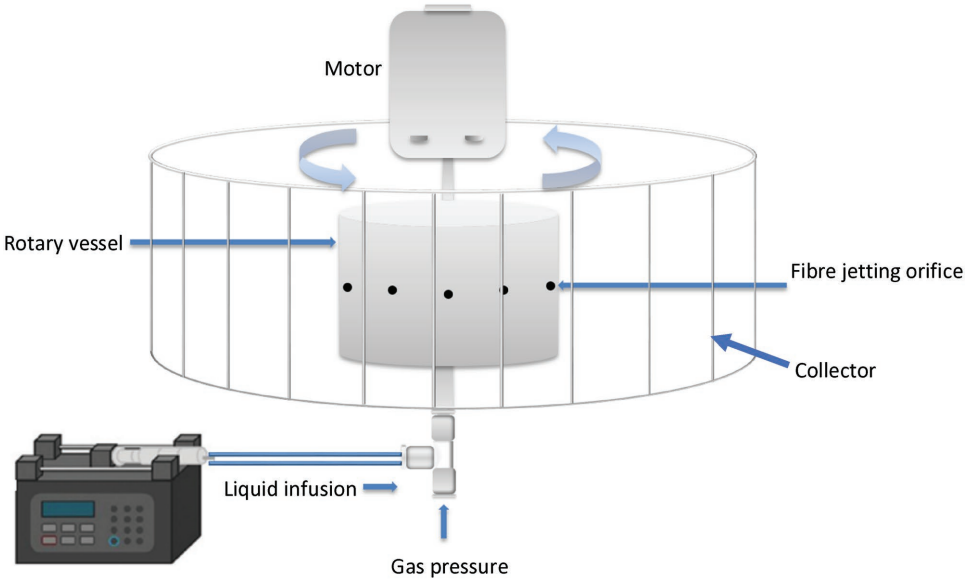

Figure 1. Schematic diagram illustrating pressure coupled infusion gyration equipment used in this work.

5000 μL min^{-1}) to investigate different scenarios. A circular copper mesh collector that surrounds the rotational vessel and was centrally placed (Figure 1), was used to collect fibers ejected from the orifices of the vessel. After collection, the fibers were covered, dried, and stored. The distance between the orifices and the circular collector was adjusted between 4 and 15 cm. PEO nanofibers with controlled morphology were produced by selective combinations between different processing parameters, including polymer concentration, rotational speed, applied pressure, infusion (flow) rate of material (polymer solution) into the vessel, and the distance at which the nanofibers (product) is collected. In order to investigate how the working parameters of PCIG affect the fiber morphology and to study the comparative performance with previous gyration methods, all polymer solutions were spun at the ambient conditions of 25 °C and 38.5% relative humidity.

Monochrome videos (12 bit) that show PCIG in action are included in the Supporting Information. These videos were recorded by a Photron Version SA1.1 high speed camera, with the help of a powerful light-emitting diode (LED) floodlight. Both low and high magnifications were used, and the recording frame rate was set at 54 000 fps. Video S0 (Supporting Information) illustrates the process.

2.3. Fiber Characterization

The morphology of produced nanofibers was characterized using field-emission scanning electron microscopy (JEOL JSM6310F). Samples were sputtered with gold-palladium using a sputter machine (Quorum Q 150R ES) for 120 s before examination. Both low and high-magnification images were taken at randomly selected positions (≈10) within each sample. By using IMAGE J software, the average fiber diameter was determined based on the mean value of ≈100 measurements analyzed from different locations per sample. The fibers were not perfectly uniform along the length in some instances, however as the number of measurements were high this does cause a dramatic influence on the results. The Gaussian distribution was plotted and fitted based on the measurement results.

2.4. 2D Fast Fourier Transform Analysis

Anisotropic alignment of nanofibers characterized by scanning electron microscopy was assessed using 2D FFT analysis. Before this analysis, uncompressed scanning electron microscope (SEM) images at the most suitable magnification were used in the quest to preserve quality, and were cropped (512 × 512 pixels dimension), and de-speckled where necessary. The 2D FFT analysis converts the information of spatial domain into a mathematically defined frequency distribution that maps the rate of change of pixel intensity across the original data image.[35,36] This output image also contains quantitative information (grayscale pixels that are distributed in a pattern) concerning the degree of fiber orientation in the data image. Thereafter, the resultant grayscale pixels distribution was used to measure pixel intensity across 360° by applying radial summation using the Oval Profile Plot Plug-in (William O'Connell) of Image J software.[37,38] Normalization of images selected from the original radial summation data set was carried out. The plots of a line graph according to the summed pixel intensity at each related acquired angle were obtained at the normalized FFT alignment with the acquisition degree. The line graph shows the relative distribution of the area of interest along angles of acquisition. The degree of alignment in these plots is reported by the height and shape of the peak.

3. Results and Discussion

3.1. Solution Viscosity

The formation and morphology of produced fiber is affected by the fluid properties, for example, viscosity of solution, which can be typically adjusted by manipulating

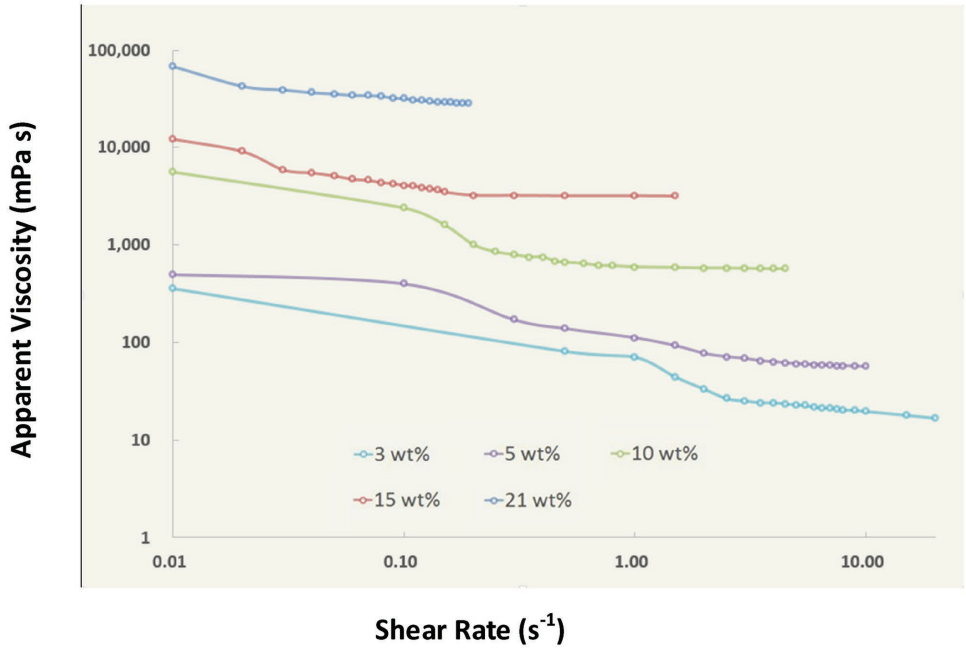

Figure 2. Flow curves of apparent viscosity–shear rate for the PEO solutions used in this work.

polymer concentration, molecular properties (structure and weight), and temperature, selectively. The flow curves (Figure 2) indicate the obvious shear thinning effects in the viscosity measurements for the prepared polymer solutions. Table 1 gives the details of the fitted power law of ($\eta = K\dot{\gamma}^{n-1}$) to the viscosity–shear rate data shown in Figure 2, where η is the measured apparent viscosity, $\dot{\gamma}$ is shear rate, and K and n are constants. The associated coefficients of multiple linear regressions ($R^2 \approx 1$) indicated high multilinear dependencies between measured viscosities and shear rates, and the dimensionless flow behavior index n elucidates obvious shear thinning effects for more viscous solutions, for example, 21 wt%. The zero shear viscosity of solutions increased from 500 to 89 500 mPa s as the polymer concentration increased from 3 to 21 wt%.

3.1.1. Effects of Infusion Rate

In pressure coupled infusion gyration, a hydrostatic pressure exists at the orifices, which is constant for a fixed flow rate, a fixed working pressure, and the rotational speed. The hydrostatic pressure will be enhanced with the increase in infusion rate. However, the hydrostatic force is much smaller when compared to the governing centrifugal force. Hence, the process of formation of nanofibers could be simply explained as a balance between surface tension force of polymer solutions and external forces (gravitational force and centrifugal force). During the spinning action, initially a steady and continuous polymer solution flow is constantly injected from the bottom of rotational vessel using a syringe pump (Figure 1). Then, the Marangoni effects due to a gradient of surface tension force across the liquid–air interface of the polymer drop emerging from the vessel orifices occurs. This leads to mass transfer of solution to the tip of the drop which forms the polymer jet.[3] This jet further elongates due to the centrifugal force and the pressure difference at the orifice. Finally, solvent evaporation takes place, thus in turn the ejected polymer jet thins and solidifies to form nanofibers.

Table 1. Fitted power law for apparent viscosities in Figure 2.

Polymer concentration [wt%]	Trend line equation	R^2	n
3	$y = 49.351x^{-0.44}$	0.9	0.56
5	$y = 111.61x^{-0.40}$	0.8	0.60
10	$y = 676.68x^{-0.34}$	0.8	0.66
15	$y = 2498.5x^{-0.26}$	0.9	0.74
21	$y = 18109x^{-0.24}$	0.9	0.76

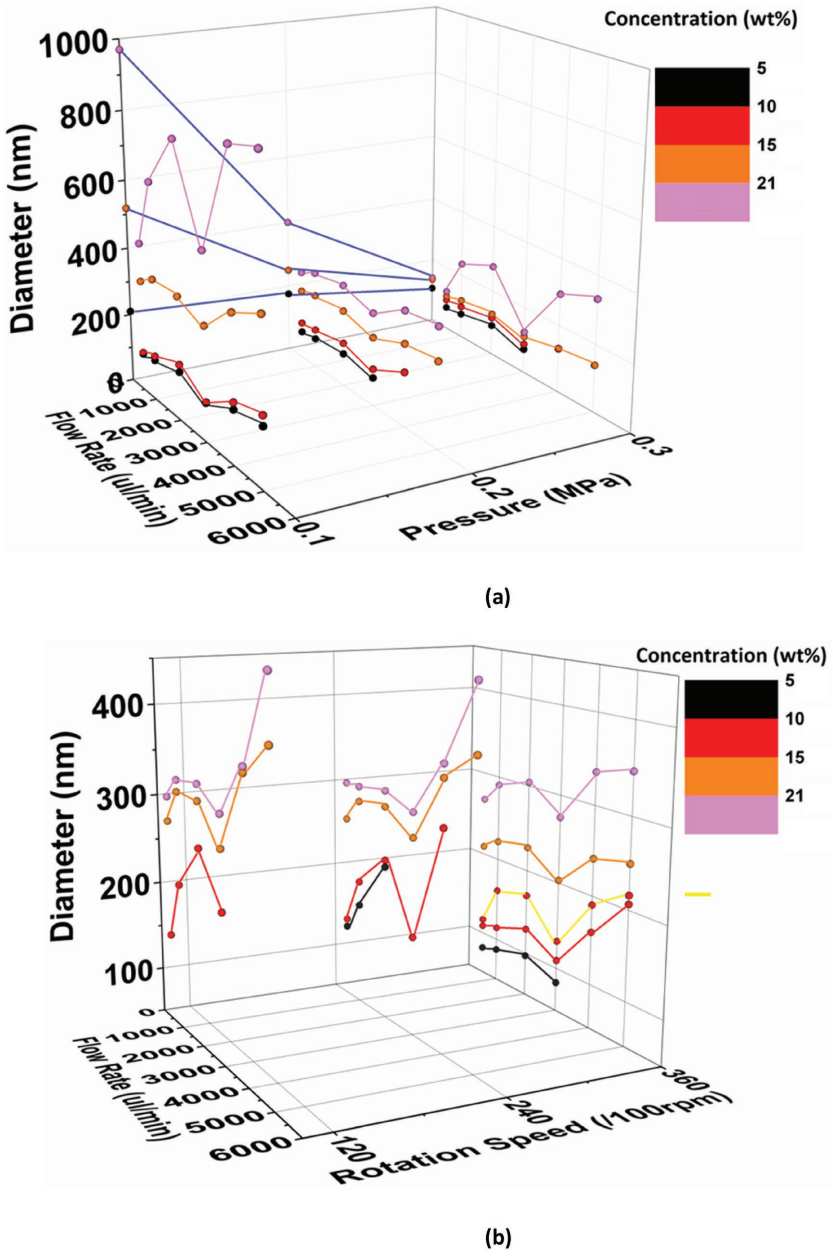

Figure 3. Combined effects of infusion rate and a) pressure and b) rotational speed on mean fiber diameter.

The combined effect of working pressure, rotational speed, and infusion rates on fiber size were correlated and are presented in Figure 3a,b. It was experimentally observed that the 3 wt% solution could not be spun into fibers and therefore produced droplets during spinning. The critical polymer concentration and chain entanglement is of crucial importance.[39–41] The critical polymer concentration for chain entanglement for our PEO can be estimated using the intrinsic viscosity of our PEO[25] and its estimation for PEO using the method of Barnes et al.,[42] and is ≈0.7 wt%. Although this approximate value is <3%, it is the closest to the critical polymer concentration value and this is probably why no fibers are obtained. For 5–21 wt% solutions, fibers were generated and the fiber diameter increased with the increase of concentration at fixed infusion rate, working pressure, and rotational speed. However, the increase of shear viscosity (Figure 2) helps in the interlocking and movement of polymer chains and how these features control jet formation and results in the evolution of fibers in gyratory forming is explained in our previous work.[43]

Figure 4a–l shows the scanning electron microscopy images and size distributions of spun fibers using 5 and 21 wt% solutions subjected to 36 000 rpm and 1×10^5 Pa. It is seen that, in general, wider size distributions are obtained at lower infusion rates. The polydispersity is 42%, 33%, 31%, 48%, 32%, and 30% for 5 wt% solution at 500–5000 μL min^{-1} flow rate. For the 21 wt% solution, a polydispersity of 53%, 45%, 42%, 50%, 45%, and 24% is found for 500–5000 μL min^{-1} flow rate. The mean fiber size ranged from 108 to 885 nm for the 5–21 wt% solutions at six different infusion rates studied. The average fiber diameters are listed in Table 2. At fixed (1×10^5 Pa) pressure and 36 000 rpm rotational speed, increasing the infusion rate showed a trend of increasing average fiber size. This is attributed to the volume and mass of polymer solution that is being transferred across the orifice which is governed by infusion rate, hence thicker polymer jets were formed (Video S1, Supporting Information) at a higher infusion rate (5000 μL min^{-1}), compared with 2000 μL min^{-1}, for 10 wt% solution at 1×10^5 Pa and 36 000 rpm. Moreover, the higher polymer concentration which, on the other hand, hinders the evaporation of solution, causes a larger transfer rate of solution across the vessel orifices. Thus, a higher flow rate leads to a lower relaxation time/evaporation during stretching of polymer jet before collection.[32] This resulted in formation of coarser fibers. Surprisingly, a drop of average fiber diameter was observed at the flow rate of 3000 μL min^{-1} for all solutions, and it subsequently increased when increasing the infusion rate further. It is

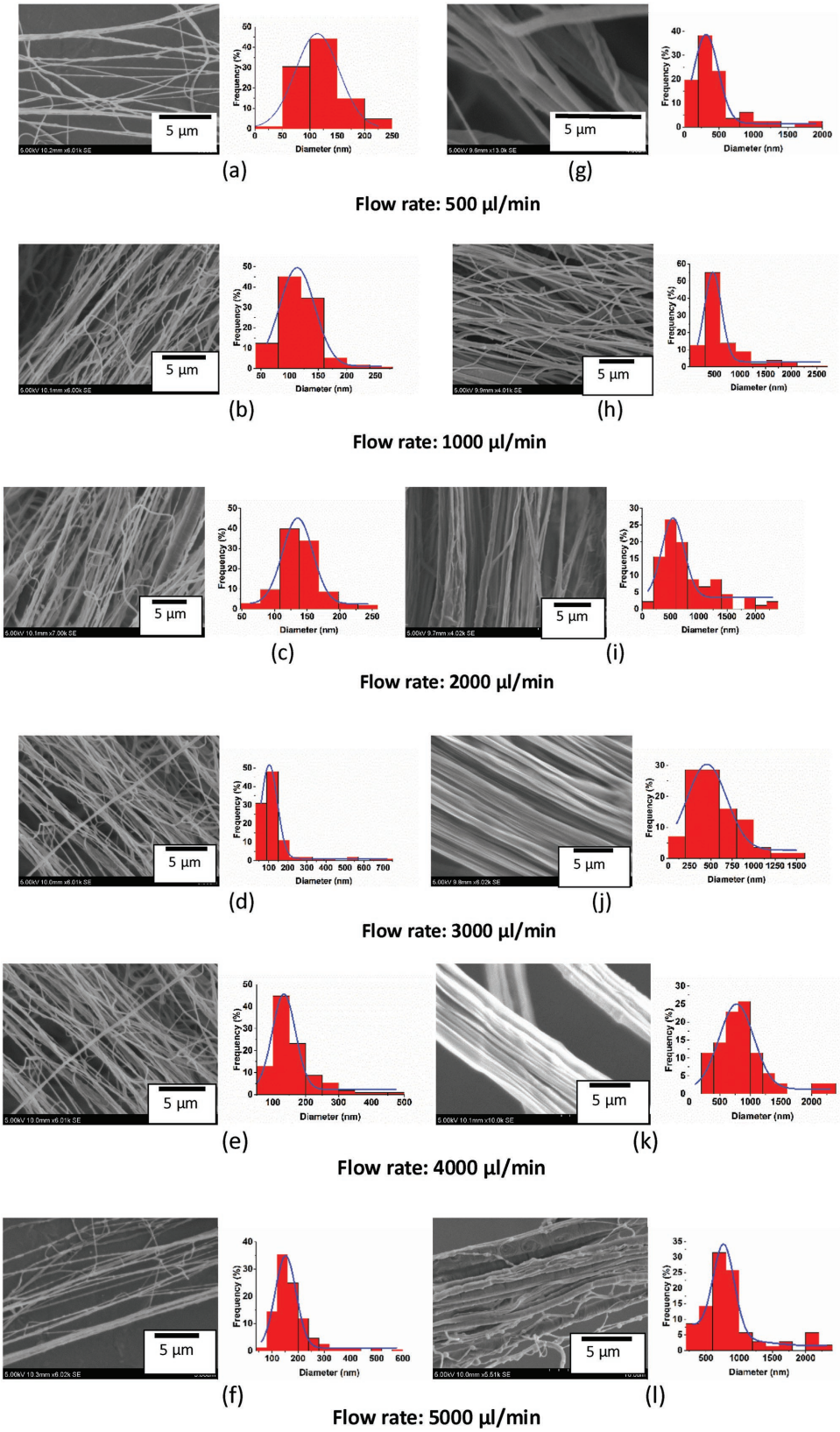

Figure 4. SEM images and fiber diameter distributions of PEO fibers produced at 500–5000 μL min^{-1} (exact relevant value indicated as shown), 36 000 rpm and 1×10^5 Pa: a–f) 5 and g–l) 21 wt%.

Table 2. Average fiber diameter (nm) at different infusion rates, 1×10^5 Pa pressure and 36 000 rpm rotational speed.

Polymer concentration [wt%]	5	10	15	21
Flow rate [μL min^{-1}]				
500	108	112	326	438
1000	118	130	357	637
2000	142	164	360	795
3000	114	116	331	538
4000	158	178	422	859
5000	177	206	473	885

believed that, this is due to a balance of volume of solution transfer through the vessel orifice operating in competition with other working parameters such as infusion rate and working pressure.

3.1.2. Effects of Working Pressure

The influence of pressure applied during gyration in generating different fiber morphologies was studied by fixing the rotational speed at 36 000 rpm and conducting experiments at 1×10^5, 2×10^5, and 3×10^5 Pa for 5–21 wt% solutions (Table 3). It is evident that, in general, a narrow distribution of fiber diameter is achieved at higher working pressures. The fiber size distributions in Figure 5a–f give polydispersities of 31%, 29%, and 43% for 10 wt% solution at 1000, 2000, and 3000 μL min^{-1} flow rate and 1×10^5 Pa pressure. It also shows polydispersity of 36%, 34%, and 40% for 3×10^5 Pa pressure for the same range of infusion rate. Table 3 shows the product geometry for the four different solutions at various pressures and flow rates. The shaded areas in Tables 3–5 indicate that droplet (black) and bead-on-string structures (gray) were formed during experiments. At any fixed polymer concentration, by increasing the pressure, a trend of reduction in the fiber diameter was observed. This is due to the introduced gas stream which enhances the combined shearing force (consisting of centrifugal force and blowing) against the surface tension force in the elongational flow of polymer jets,[3] and therefore reduces the diameters of the ejected polymer jets at the orifices of vessel, which helps to promote thinner fiber formation (Video S2, Supporting Information). Solvent evaporation can be enhanced by blowing which affects the relative speed of gas flow on the liquid–air interface in the polymer drops and solvent diffusion across polymer drops to the surface, thus contributing to fiber formation.

Table 3. Average fiber diameter (nm) obtained at different pressures, for various infusion rates, and 36 000 rpm rotational speed. The shaded areas indicate that droplet (black) and bead-on-string structures (gray) were formed.

Polymer concentration [wt%]	5	10	15	21	Working pressure [Pa]
Flow rate [μL min^{-1}]					
500	108	112	326	438	1×10^5
	81	108	209	268	2×10^5
	68	92	105	121	3×10^5
1000	118	130	357	637	1×10^5
	87	114	222	291	2×10^5
	73	97	117	236	3×10^5
2000	142	164	360	795	1×10^5
	97	129	227	324	2×10^5
	90	114	127	276	3×10^5
3000	114	116	331	538	1×10^5
	83	109	203	275	2×10^5
	71	87	111	124	3×10^5
4000	158	178	422	859	1×10^5
		159	242	336	2×10^5
		130	139	294	3×10^5
5000	177	206	473	885	1×10^5
			250	347	2×10^5
				332	3×10^5

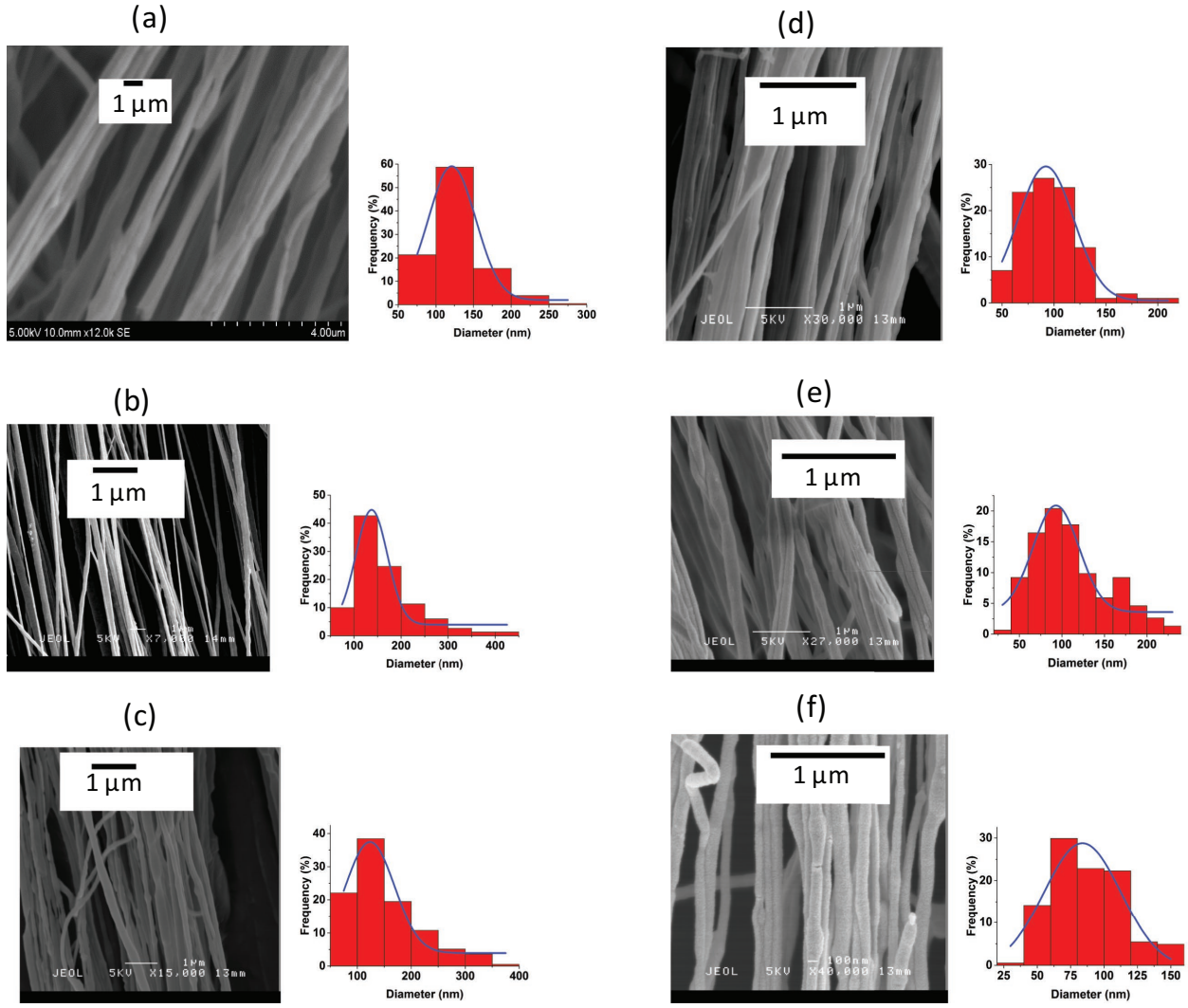

Figure 5. SEM images and diameter distributions of the products for 10 wt% PEO solution at a–c) 1×10^5 and d–f) 3×10^5 Pa, 1000, 2000, and 3000 µL min^{-1}, 36 000 rpm.

For 2×10^5 Pa pressure, the 5 wt% solution gave uniform fibers at flow rates of 500–3000 µL min^{-1}, and a bead-on-string structure was formed when the flow rate was increased to 4000 and 5000 µL min^{-1} (Figure 6a,b). The size of beads spanned a range of dimensions, which gave 58–201 and 157–350 nm in width and 64–202 and 173–370 nm in length, respectively. When the working pressure was increased to 3×10^5 Pa, the bead-on-string formation was enhanced at the flow rate of 4000 µL min^{-1}, that is, larger beads size and wider size range of beads were obtained. There was no product to collect except droplets at a flow rate of 5000 µL min^{-1}. The same trend was also found with the 10 wt% solution. Figure 6d shows that coarser fibers were formed at flow rate of 3000 µL min^{-1} and 2×10^5 Pa pressure. Figure 6e,g shows the fibers obtained at 4000 µL min^{-1} and working pressure of 2×10^5 to 3×10^5 Pa, respectively. Bead-on-string structure was formed rather than droplets at 5000 µL min^{-1} with a pressure of 2×10^5 and 3×10^5 Pa. The range of bead width is 167–371, 192–373, and 201–400, 217–471 nm in length, for pressure of 2×10^5 and 3×10^5 Pa, respectively. During the spinning action, the introduction of gas enhances the instability of polymer jets at the jetting orifices which helps to promote beads formation. It also facilitates solvent evaporation which takes place in the radial direction of jets. The results also indicate that the polymer concentration has significant influence on the as-spun fiber morphology, that is, the increased polymer viscosity plays a role of stabilizing polymer jets against the action of centrifugal force and dynamic solution blowing, hence promoting larger bead size and fiber diameter. The morphology of beads for 15 wt% solution at 5000 µL min^{-1}, 3×10^5 Pa shows a spindle-like shape compared to the spherical

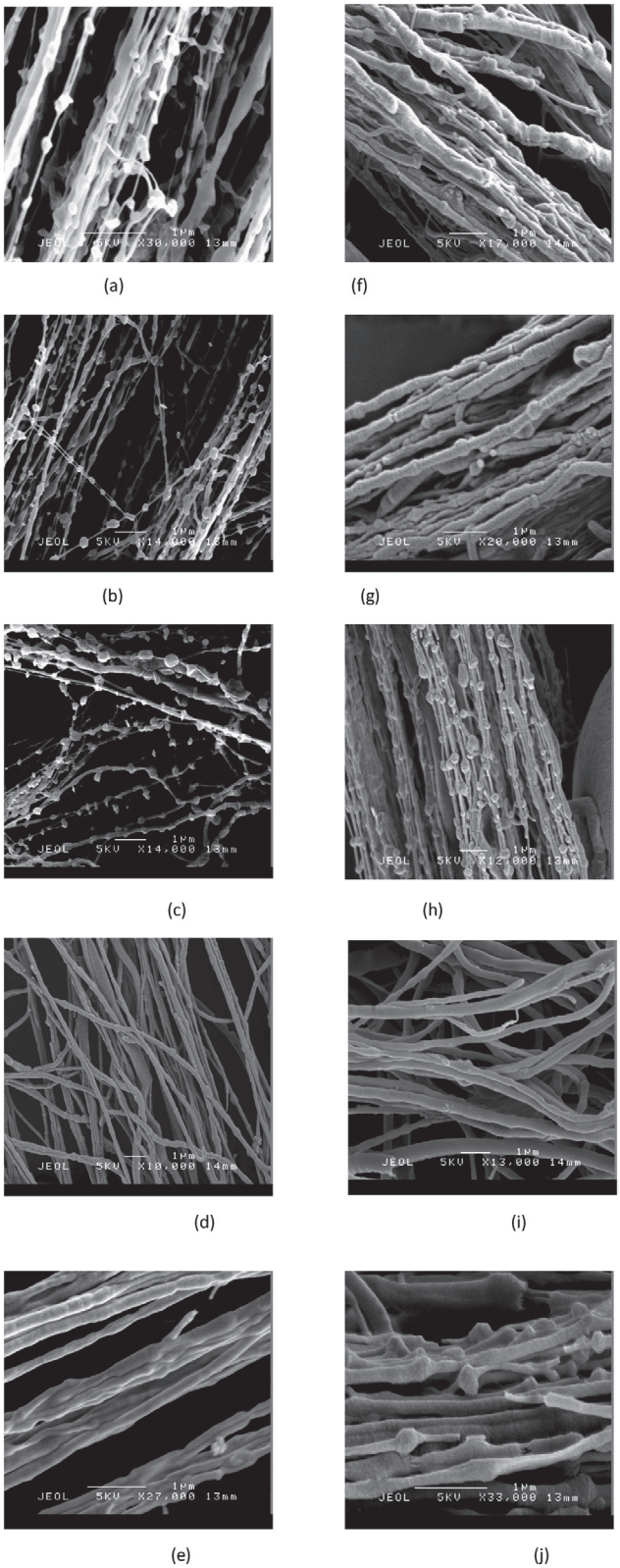

Figure 6. Fibers and bead-on-string structures produced at 36 000 rpm speed: a,b) bead-on-string structure from 5 wt% solution at 2×10^5 Pa pressure, 4000–5000 µL min^{-1} flow rate; c) bead-on-string structure from 5 wt% solution at 3×10^5 Pa pressure, 4000 µL min^{-1} flow rate; d,e) coarser fiber from 10 wt% solution at 2×10^5 Pa pressure, 3000–4000 µL min^{-1} flow rate; f,h) bead-on-string structure from 10 wt% solution at 2×10^5 and 3×10^5 pressure, 5000 µL min^{-1} flow rate; g) coarser fiber from 10 wt% solution at 3×10^5 Pa pressure, 4000 µL min^{-1} flow rate; i) uniform fiber from 15 wt% solution at 3×10^5 Pa pressure, 4000 µL min^{-1} flow rate; j) bead-on-string structure from 15 wt% solution at 3×10^5 Pa pressure, 5000 µL min^{-1} flow rate.

beads generated at 5 and 10 wt% solutions. The bead size also increased, which gave 152–368 nm width and 226–565 nm length. When the polymer concentration is continuously increased, bead formation finally disappeared as observed with the 21 wt% solution. This can be attributed to the higher polymer concentration which hinders solvent evaporation, hence it leads to relatively longer relaxation time/evaporation time during stretching. In addition, there are large size differences between some of the adjacent beads as formed in several SEM images in this study, for example, Figure 6h. It occurs because of the stretching phenomenon caused by the instability and elastic recoil takes place at the neck region formed between bead and fiber. It is probably a balance between inertia, capillarity, and viscoelasticity of the polymer solution.[44–47]

Compared with typical pressurized gyration[3] (Table 4 and Figure 3a) the fiber produced using PCIG was much thinner. This is because the dynamic fluid flow can be regulated by infusion rate of solution when flowing across orifice during spinning, hence the material input could be effectively used and obtaining the desired product morphology be achieved by balancing different combinations of processing parameters with solvent evaporation. Although less obvious, the results in Figure 3b also indicate an enhanced thinning effect due to the result of a higher shear force provided by gas blowing, when compared with infusion gyration. Full details of comparison of produced fiber size are shown in Table 5. Infusion also has the advantage of preventing the loss of prefilled material during initial acceleration in order to reach the desired rotating speed.

3.1.3. Effects of Rotational Speed

Similar to pressurized gyration, the basic governing forces in PCIG spinning consist of centrifugal force and dynamic fluid flow. The combination of solution blowing and centrifugal force against the surface tension force leads to deformation of polymer droplets and thus enables fiber formation from the vessel orifices. In general, this deformation will be enhanced by higher centrifugal force provided by a higher rotational speed. The normal stresses in contrast to shear stresses in non-Newtonian fluid exist, and causes the stresses to act in the same direction as

Table 4. Comparison of results (nm) of pressure coupled infusion gyration and typical pressurized gyration. The black shaded areas indicate that droplets were formed.

Polymer concentration [wt%]	5	5 (PG)[a)]	15	15 (PG)	21	21 (PG)	WP[b)] [Pa]	RS[c)] [rpm]
Flow rate [μL min^{-1}]								
500	108	210	326	518	438	970	1×10^5	36 000
	81	175	209	250	268	400	2×10^5	36 000
	68	106	105	135	121	141	3×10^5	36 000
	131		260	560	302	600	2×10^5	24 000
			276		303	692	2×10^5	10 000
1000	118		357		637		1×10^5	36 000
	87		222		291		2×10^5	36 000
	73		117		236		3×10^5	36 000
	164		286		303		2×10^5	24 000
			314		327		2×10^5	10 000
2000	142		360		795		1×10^5	36 000
	97		227		324		2×10^5	36 000
	90		127		276		3×10^5	36 000
	223		291		309		2×10^5	24 000
			315		333		2×10^5	10 000
3000	114		331		538		1×10^5	36 000
	83		203		275		2×10^5	36 000
	71		111		124		3×10^5	36 000
			160		297		2×10^5	24 000
			213		314		2×10^5	10 000

[a)]PG = pressurized gyration; [b)]WP = working pressure; [c)]RS = rotational speed.

the deformation plane.[3] Thus, the stretched polymer jets will be accelerated by the centrifugal force and further enhanced by gas blowing.

The change in rotation speed during spinning determines the final fiber diameter. The viscosity of solution can vary during spinning due to a temperature gradient which can occur through the polymer jets during the solvent evaporation. Mahalingam and Edirisinghe[3] have indicated that the time constant of shearing forces applied on polymer jets during pressurized gyration will be decreased with increasing rotation speed. In addition, the time constant of shearing forces governs the responses of polymer chains, that is, higher the time constant the longer the viscous response of polymer solution, and vice versa. Hence, a minimum rotation speed that could result in enough viscous solution response enables the generation of nanofibers at lower polymer concentrations.

To identify the correlation between the fiber morphology and rotational speed, the 5–21 wt% solutions were spun at a fixed working pressure of 2×10^5 Pa and the rotational speed and infusion rate were varied. A definite relationship between polymer concentration, rotational speed, infusion rate, and fiber diameter is clearly seen in Table 5. For comparison, the results obtained at 36 000 rpm rotational speed and 2×10^5 Pa pressure is also listed here. On the whole, increasing rotational speed accelerates stretching of polymer jets, this decreases the diameters of the polymer jets at the orifices of vessel and thinner fibers are obtained (Figure 7a–f and Video S3, Supporting Information). The 15 wt% solution gave 276 and 260 nm in diameter at 10 000 and 24 000 rpm at the same infusion rate of 500 μL min^{-1}, and 399 and 376 nm in diameter at 10 000 and 24 000 rpm at an infusion rate of 5000 μL min^{-1}. It is clearly seen that, overall, a narrower size distribution is obtained at a higher rotational speed. For the 15 wt% solution, for fixed 2×10^5 Pa pressure, the polydispersity is 40%, 37%, and 47% for a lower rotational speed (10 000 rpm) and flow rate values of 1000, 2000, and 3000 μL min^{-1}; the polydispersity is 36%, 34%, and 45% for a higher rotational speed (36 000 rpm) with the

Table 5. Average fiber diameters (nm) obtained at different rotational speeds and infusion rates, in all cases pressure was 2×10^5 Pa. The shaded areas indicate that droplet (black) and bead-on-string structures (gray) were formed.

Polymer concentration [wt%]	5	10	10 (IG at 0 pressure)[a)]	15	21	RS[b)] [rpm]
Flow rate [μL min^{-1}]						
500		147		276	303	10 000
	131	140		260	302	24 000
	81	108	117	209	268	36 000
1000		212		314	327	10 000
	164	192		286	303	24 000
	87	114	161	222	291	36 000
2000		266		315	333	10 000
	223	231		291	309	24 000
	97	129	170	227	324	36 000
3000		213		278	314	10 000
		160		269	297	24 000
	83	109	132	203	275	36 000
4000				365	370	10 000
		292		344	358	24 000
		159	190	242	336	36 000
5000				399	466	10 000
				376	448	24 000
			216	250	347	36 000

[a)]IG = infusion gyration; [b)]RS = rotational speed.

same range of flow rates. It is noteworthy that, 5 wt% solution is not spinnable using a typical pressurized gyration method at pressure of 2×10^5 Pa and rotational speed of ≤24 000 rpm. However, this new process enables gyratory spinning of these and this is also true for the 15 wt% solution processed at a pressure of 2×10^5 Pa and a rotational speed of 10 000 rpm. This is due to regulated mass transfer of polymer solution through the orifice by controlled infusion.

3.1.4. Analysis of Fiber Anisotropy

FFT analysis of SEM images was used to characterize the scaffold anisotropy and degrees of fiber alignment. It is possible to assess the impact of various processing parameters on the product morphology by FFT to assign a relative alignment number to a spun matrix. FFT is a rapid method for assessing fiber alignment in tissue-engineering materials.[36] In this analysis, the degree of fiber alignment in a line chart is represented by the height and shape of the peak compiled statistics from FFT graph (Figure 8). The more uniformly orientated fibers will offer a more spindle-like shape in a frequency graph that could be related with the overall orientation of fibers in the original SEM images. The sharper peaks, that is, the detected pixel intensities in the frequency graph, for example, Figure 8c, are in a single direction. The more randomly orientated fibers will provide circular shape at the center of the plotted frequency graph, and broader peaks with relative lower amplitude.[36] The broader peaks with low amplitude were caused by background noise, and the distinct pointed peaks at single specific values were induced by edge effects in most case, which can be removed manually. PCIG products spun from a starting concentration of 10 wt% exhibit overt evidence of alignment at any infusion rate, rotational speed, and gyration pressure and thus give rise to bead-on-string structures or fibers.

Statistical analysis indicates that fibers produced from 10 and 15 wt% solutions at fixed rotational speed (36 000 rpm) showed uniform fiber alignment and smooth surface roughness (Figures 5 and 7). Both peak height and width of curves represent the relative degree of fiber alignment, and the position of peak shows the principle axis of fiber orientation in the related SEM images. In Figure 8a–h, higher peaks were obtained at higher infusion rates. The 10 wt% gave 0.17–2.20 units of alignment, and the 15 wt% gave 1.60–3.02 units of alignment when increasing the

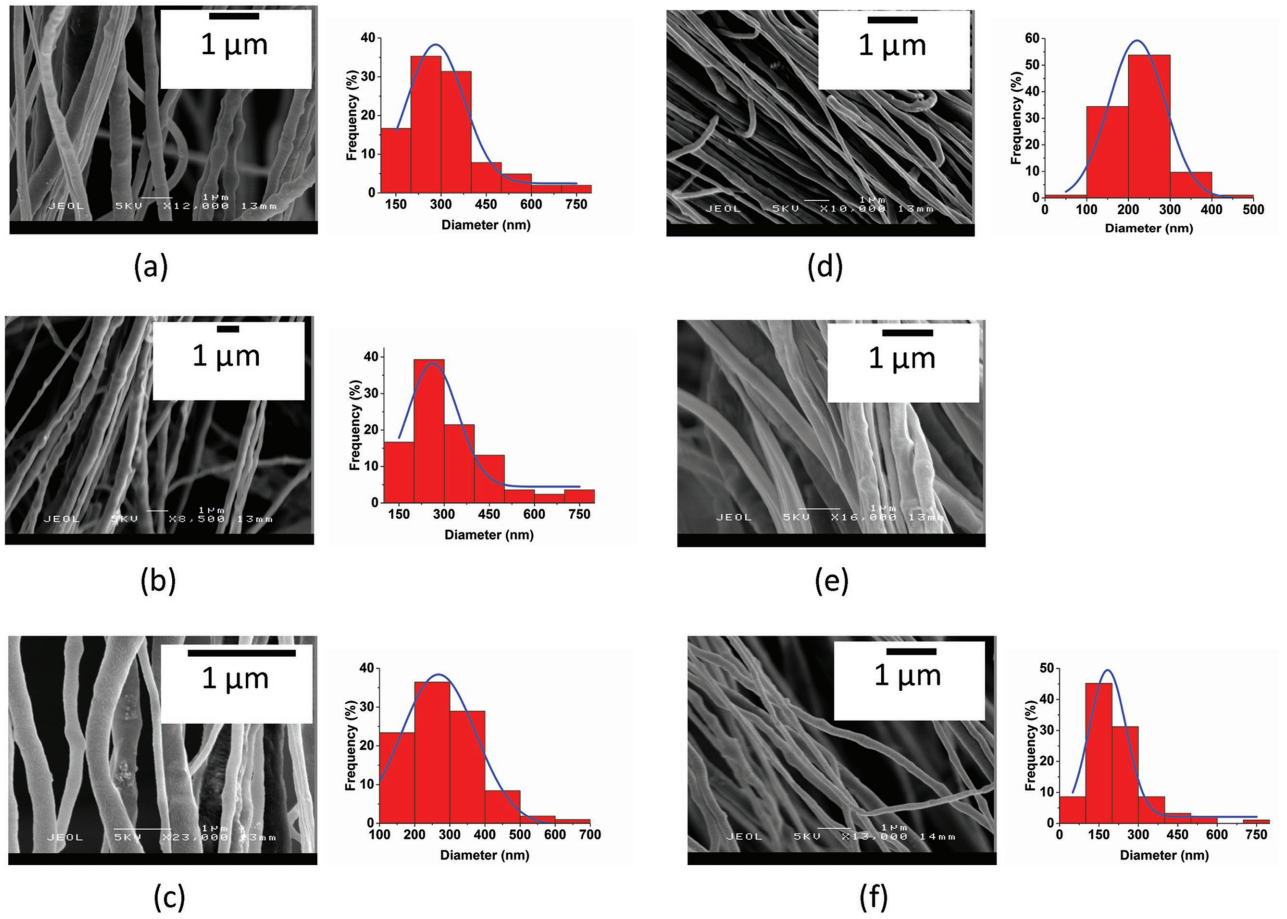

Figure 7. SEM images and diameter distributions of the products for 15 wt% PEO solution at 2×10^5 Pa, 1000, 2000, and 3000 μL min^{-1}, and different rotational speed: a–c) 10 000 and d–f) 36 000 rpm.

infusion rate from 2000 to 5000 μL min^{-1} at a fixed rotational speed and a pressure of 1×10^5 Pa. In addition, loose alignments were obtained at 3000 μL min^{-1} for both solutions (Figure 8b,f,j). This is because the fiber mat consists of thicker fibers and was more stable so that it could retain the structures during transit and before reaching the collector. Wide and shoulder-like peaks with almost same amplitude can be induced (Figure 8j), and indicates part of the fibers deviated from the overall orientation of the fiber mat. Comparing the subpeaks brought by background information and noise, the relative broader subpeaks in Figure 8i can be attributed to the random elements. For instance, the beads formed in 15 wt% in the original SEM image are shown in the frequency of pixel intensity which could be assigned to any angle within 360°.[48]

Width of FFT alignment peaks for fibers prepared from the 10 and 15 wt% solutions sequentially decreased as a function of infusion rate and rotational speed, however it increased as a function of working pressure. In contrast, broader peaks and relative lower alignment values (1.35–2.07) can be assigned to fibers produced at 0.3 MPa (Figure 8i–l). Furthermore, the fibers generated from the 10 wt% PEO solution were relatively loosely aligned compared with the fibers produced from the 15 wt% solution. This may be attributed to the higher viscosity of 15 wt% solution which is relatively easier to spin compared to the 10 wt%.

3.1.5. Effect of Collection Distance

In PCIG, determining the appropriate distance for fiber collection is based on the type of collector, the required diameter of spiral trajectory of polymer jets, and the duration of solvent evaporation. The travelling time of polymer jets is solely decided by orifice-to-collector distance. For any type of spinning dope, a selective minimum critical distance between the orifice and collector is related to the critical time of the solvent evaporation. If the orifice-to-collector distance is relatively short, the fiber will not be elongated enough before reaching the collector. This will result in thicker fibers. On the other hand, the effect of collection distance on fiber morphology can have a negligible effect, if it is beyond the critical value, as explained before.

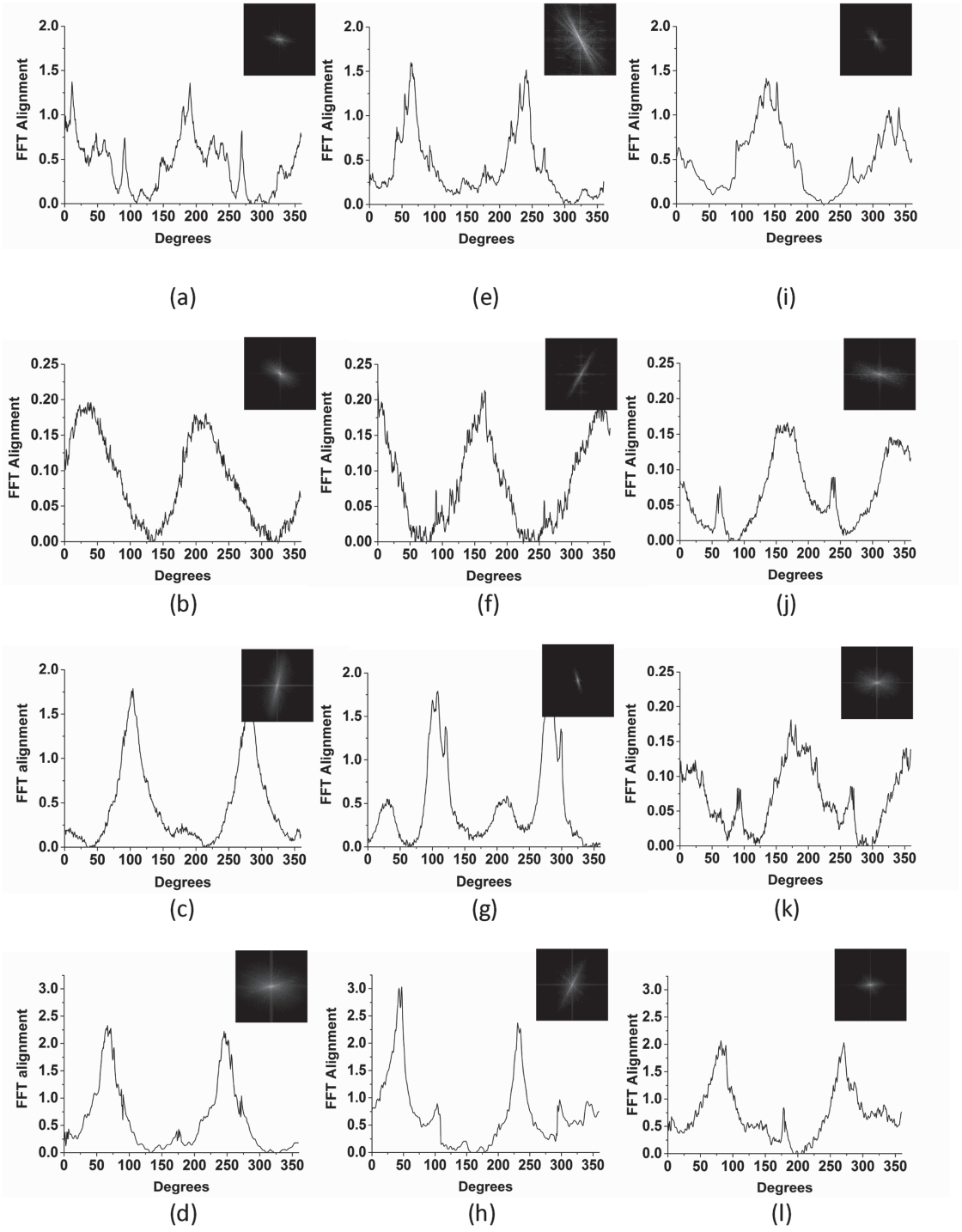

Figure 8. 2D FFT alignment analysis of fibers: a–d) 10 wt% solution, e–h) 15 wt% solution at 2000, 3000, 4000, and 5000 μL min^{-1} infusion rate, 36 000 rpm rotational speed, and 1×10^5 Pa; i–l) 15 wt% solution at 0.3 MPa, the same range of infusion rate and the rotational speed as in (e)–(h).

Figure 9a–e shows SEM images and size distributions of nanofibers spun at different orifice-to-collector distances: 4, 5, 7, 10, and 15 cm, with a 5000 μL min^{-1} infusion rate, rotational speed of 36 000 rpm, and 0.1 MPa working pressure. The results here indicate that wider diameter distributions of fibers were obtained at lower collection distances, for example, 4 and 5 cm; the polydispersity index is 33% and 31% for a collection distance 4–5 cm; the polydispersity is 29%, 25%, and 29% for 7–10 cm. In Figure 9a, it is clearly seen that the morphology of 21 wt%

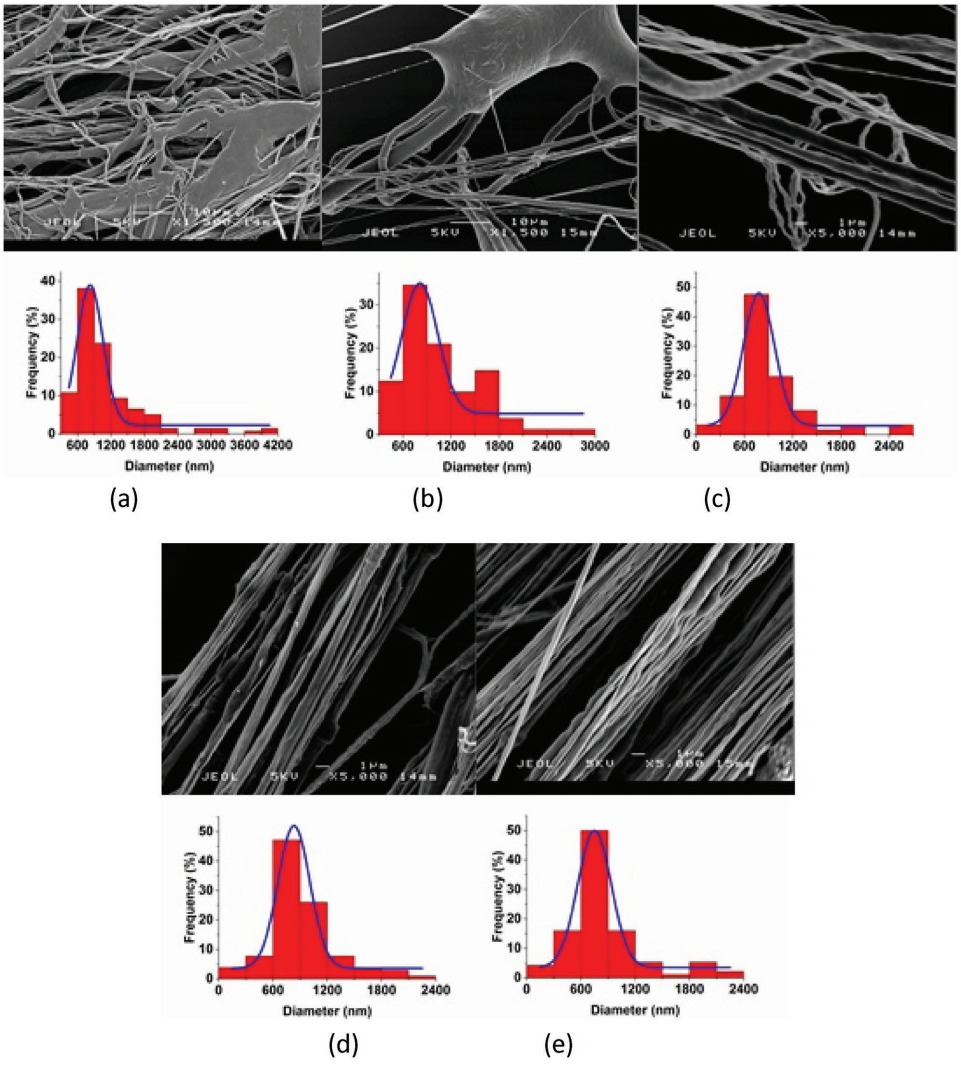

Figure 9. Fibers of 21 wt% solution obtained at 5000 μL min^{-1} flow rate, 36 000 rpm speed, 1×10^5 Pa pressure and collection distance of a) 4, b) 5, c) 7, d) 10, and e) 15 cm.

PEO solution at 4 cm collection distance shows severely agglomerated fibers (1118 nm) to form joint blocks. This is due to the process generating a polymeric web in very short duration and insufficient solvent evaporation of polymer jets before they reach the collector leading to accumulation of fibers in the vicinity. This phenomenon was slightly improved at 5 cm, the density of "joined fibers" decreased and the averaged fiber diameter was 1088 nm.

When increasing the distance to 7 and 10 cm, the product morphology was improved, finer fibers without joined blocks were obtained (Figure 9c,d and Video S4 of Supporting Information). The produced fiber diameter at 7 and 10 cm was measured and found to have a negligible difference, that is, 898 and 900 nm, respectively. When continuously increasing the orifice-to-collector distance to 15 cm, the average fiber diameter exhibits insignificant change (888 nm at 15 cm). This elucidates that there is a need to have a minimum collection distance in the pressure coupled infusion gyration method to allow sufficient solvent evaporation in the polymer jets. The results show that the solvent has been sufficiently evaporated at 7 cm orifice-to-collector distance, and further evaporation of solvent of polymer jet is attributed to the extension of collector distance to 10 and 15 cm. When compared with other processing parameters, the effect of orifice-to-collector distance above 7 cm had a minimal effect on the product morphology. With the 21 wt% PEO solution decreasing the distance to 3 cm was attempted, but there was no product to collect except polymer droplets.

The production yield of fibers of PCIG will depend on the interaction of the three process control parameters—rotational speed, pressure, and flow rate. Our previous

work[3,32] has indicated how the yield will vary when pressure and flow rate were independently varied at a rotation speed. In particular, with infusion gyration[32] where flow rate was varied, significant improvement in yield was not seen until a flow rate of 5000 μL min^{-1}. Many phenomena take place in the vessel prior to the ejection of fibers from the orifices. Previous work on pressurized gyration[3] and our ongoing research suggest that fibers are generated by the breakup of a blob of polymer at the orifice. Also, rotation can involve the formation of a vortex in the vessel and evaporation of solvent leading to a more concentrated polymer solution from which fibers evolve. Thus, the flow may not be continuous with respect to the initial polymer solution fed into the vessel. The above-mentioned scenarios are being investigated in our laboratory at present.

4. Conclusions

An effective and simple PCIG system has been developed to produce polymeric fibers. Using a PEO–water system we demonstrate that fibers in the range of 60–850 nm can be mass produced. Compared with other existing spinning methods, it is inexpensive, easy to be deployed, and has relatively lower requirements for properties of spinning dope. It inherits the benefits from typical pressurized gyration and infusion gyration, that is, it is applicable for mass production of highly well-aligned fibers along the radial direction of the spinning vessel, offering fibers with better geometry and it also extends spinnable scope for dilute solutions, for example, 5 wt% using selective combinations of parameters. The effects of processing parameters (infusion rate, working pressure, rotational speed, and collection distance) and solution concentration on product morphology were studied in detail. At fixed rotational speed and pressure, fiber diameter increased with increase in infusion rate.

When increasing working pressure, increasing infusion rate, and fixed rotational speed, droplets and bead-on-string structure appeared in the products of 5–15 wt% solutions, and this demonstrated that the enhanced pressure and infusion rate will affect the balance of polymer transfer across the vessel orifices in spinning to promote droplets and bead formation. At fixed pressure, fixed infusion rate, and changing rotational speed, the obtained fiber diameter shows a trend of increase as rotational speed decrease, and this is due to the centrifugal force being proportional to rotational speed. The orifice-to-collector distance directly affects the produced fiber morphology, as well as a minimum critical collection distance (7 cm in the present work) existed that favored obtaining desirable morphology and this value tends to be less influential once this critical value is exceeded. The method allows the product morphology to be substantially controlled by different combinations of the above-mentioned processing parameters. It is anticipated that the simplicity and versatility of this method could make it another potential way to produce nanofibers in high volume and cost effectively.

Supporting Information

Supporting Information is available from the Wiley Online Library or from the author.

Acknowledgements: The authors thank the Engineering & Physical Sciences Research Council (UK) for supporting gyratory fibre preparation research at UCL, in particular SM is supported by current EPSRC grant EP/N 034228/1. Data supporting this paper are provided in the paper and as Supplementary Information accompanying this paper.

Reference 29, reference link 32, and a spelling mistake in Figure 2 was corrected on June 16, 2017.

Received: December 22, 2016; Revised: January 20, 2017; Published online: March 27, 2017; DOI: 10.1002/mame.201600564

Keywords: gyration; infusion; manufacture; nanofiber; polymer; pressure; production

[1] G. L. Bezemer, J. H. Bitter, H. P. Kuipers, H. Oosterbeek, J. E. Holewijn, X. Xu, F. Kapteijn, A. J. van Dillen, K. P. de Jong, *J. Am. Chem. Soc.* **2006**, *128*, 3956.
[2] N. M. Rodriguez, M.-S. Kim, R. T. K. Baker, *J. Phys.Chem.* **1994**, *98*, 13108.
[3] S. Mahalingam, M. Edirisinghe, *Macromol. Rapid Commun.* **2013**, *34*, 1134.
[4] T. Maiyalagan, K. Scott, *J. Power Sources* **2010**, *195*, 5246.
[5] C. Pham-Huu, N. Keller, V. V. Roddatis, G. Mestl, R. Schlögl, M. J. Ledoux, *Phys. Chem. Chem. Phys.* **2002**, *4*, 514.
[6] K. P. De Jong, J. W. Geus, *Cat. Rev.* **2000**, *42*, 481.
[7] M. L. Toebes, F. F. Prinsloo, J. H. Bitter, A. J. van Dillen, K. P. de Jong, *J. Catal.* **2003**, *214*, 78.
[8] G. L. Bezemer, P. Radstake, V. Koot, A. Van Dillen, J. Geus, K. De Jong, *J. Catal.* **2006**, *237*, 291.
[9] Y. L. Hsin, K. C. Hwang, C.-T. Yeh, *J. Am. Chem. Soc.* **2007**, *129*, 9999.
[10] M. Shin, H. Yoshimoto, J. P. Vacanti, *Tissue Eng.* **2004**, *10*, 33.
[11] Q. P. Pham, U. Sharma, A. G. Mikos, *Tissue Eng.* **2006**, *12*, 1197.
[12] J. R. Porter, T. T. Ruckh, K. C. Popat, *Biotechnol. Prog.* **2009**, *25*, 1539.
[13] X. Xin, M. Hussain, J. J. Mao, *Biomaterials* **2007**, *28*, 316.
[14] Z. Ahmad, E. Stride, M. Edirisinghe, *J. Drug Targeting* **2009**, *17*, 724.
[15] R. Vasita, D. S. Katti, *Int. J. Nanomed.* **2006**, *1*, 15.
[16] S. V. Lomov, A. Willems, I. Verpoest, Y. Zhu, M. Barburski, T. Stoilova, *Text. Res. J.* **2006**, *76*, 243.
[17] K. Buet-Gautier, P. Boisse, *Exp. Mech.* **2001**, *41*, 260.
[18] W. Liu, S. Thomopoulos, Y. Xia, *Adv. Healthcare Mater.* **2012**, *1*, 10.
[19] S. Kumbar, R. James, S. Nukavarapu, C. Laurencin, *Biomed. Mater.* **2008**, *3*, 034002.

[20] H. Y. Zhu, J. D. Riches, J. C. Barry, *Chem. Mater.* **2002**, *14*, 2086.
[21] J. del Barrio, L. Oriol, C. Sánchez, J. L. Serrano, A. l. Di Cicco, P. Keller, M.-H. Li, *J. Am. Chem. Soc.* **2010**, *132*, 3762.
[22] C. Luo, S. D. Stoyanov, E. Stride, E. Pelan, M. Edirisinghe, *Chem. Soc. Rev.* **2012**, *41*, 4708.
[23] K. A. Rieger, N. P. Birch, J. D. Schiffman, *Carbohydr. Polym.* **2016**, *139*, 131.
[24] T. Yian, H. Hsuye, C. Jiengchiang, W. Chingshiun, *Text. Res. J.* **2011**, *32*, 17.
[25] P. Gupta, C. Elkins, T. E. Long, G. L. Wilkes, *Polymer* **2005**, *46*, 4799.
[26] R. Weitz, L. Harnau, S. Rauschenbach, M. Burghard, K. Kern, *Nano Lett.* **2008**, *8*, 1187.
[27] M. R. Badrossamay, H. A. McIlwee, J. A. Goss, K. K. Parker, *Nano Lett.* **2010**, *10*, 2257.
[28] M. A. Hammami, M. Krifa, O. Harzallah, *J. Text. Inst.* **2014**, *105*, 637.
[29] Z. Xu, S. Mahalingam, P. Basnett, B. Raimi-Abraham, I. Roy, D. Craig, M. Edirisinghe, *Macromol. Mater. Eng.* **2016**, *301*, 922.
[30] S. Mahalingam, G. Ren, M. Edirisinghe, *Carbohydr. Polym.* **2014**, *114*, 279.
[31] S. Mahalingam, B. T. Raimi-Abraham, D. Q. Craig, M. Edirisinghe, *Langmuir* **2014**, *31*, 659.
[32] S. Zhang, B. T. Karaca, S. K. VanOosten, E. Yuca, S. Mahalingam, M. Edirisinghe, C. Tamerler, *Macromol. Rapid Commun.* **2015**, *36*, 1322.
[33] Z. Xu, S. Mahalingam, J. L. Rohn, G. Ren, M. Edirisinghe, *Mater. Sci. Eng.* **2015**, *C 56*, 195.
[34] M. Orlu-Gul, A. A. Topcu, T. Shams, S. Mahalingam, M. Edirisinghe, *Curr. Opin. Pharmacol.* **2014**, *18*, 28.
[35] L. Nivison-Smith, A. S. Weiss, *J. Biomed. Mater. Res., Part A* **2012**, *100*, 155.
[36] M. Tunák, A. Linka, presented at Proc. 12th Int. Conf. (STRUTEX), Liberec, Czech Republic, Nov. 28–29, **2005**.
[37] M. Shang, W. Wang, W. Yin, J. Ren, S. Sun, L. Zhang, *Chem. Eur. J.* **2010**, *16*, 11412.
[38] A. Bassi, J. Gough, M. Zakikhani, S. Downes, *J. Tissue Eng.* **2011**, *2*, 615382.
[39] C. L. Casper, J. S. Stephens, N. G. Tassi, D. B. Chase, J. F. Rabolt, *Macromolecules* **2004**, *37*, 573.
[40] D. Petras, P. Slobodian, V. Pavlínek, P. Sáha, D. Kimmer, presented at Novel Trends in Rheology IV, July 27–28, **2011**.
[41] S. Mahalingam, G. Pierin, P. Colombo, M. Edirisinghe, *Ceram. Int.* **2015**, *41*, 6067.
[42] W. J. Barnes, F. P. Price, *J. Polym. Sci.* **1961**, *153*, S25.
[43] X. Hong, M. Edirisinghe, S. Mahalingam, *Mater. Sci. Eng., C* **2016**, *69*, 1373.
[44] H.-C. Chang, E. A. Demekhin, E. Kalaidin, *Phys. Fluids* **1999**, *11*, 1717.
[45] H. Fong, I. Chun, D. Reneker, *Polymer* **1999**, *40*, 4585.
[46] M. S. Oliveira, R. Yeh, G. H. McKinley, *J. Non-Newtonian Fluid Mech.* **2006**, *137*, 137.
[47] L. Wang, J. Shi, L. Liu, E. Secret, Y. Chen, *Microelectron. Eng.* **2011**, *88*, 1718.
[48] A. K. Gaharwar, M. Nikkhah, S. Sant, A. Khademhosseini, *Biofabrication* **2014**, *7*, 015001.